Unravelling the role of alcohol copper radical oxidases in fungal plant pathogens

Bastien Bissaro
INRAE(France) https://orcid.org/0000-0001-8354-3892
Sayo Kodama
Setsunan University
Hayat Hage
INRAE
David Ribeaucourt
INRAE
Mireille Haon
INRA
Sacha Grisel
INRAE
A Simaan
CNRS
Fred Beisson
CEA https://orcid.org/0000-0001-9995-7387
Stephanie Forget
University of British Columbia
Harry Brumer
University of British Columbia https://orcid.org/0000-0002-0101-862X
Marie-Noelle Rosso
INRAE
Richard O'Connell
INRAE
Mickael Lafond
Aix-Marseille University
Yasuyuki Kubo
Setsunan University
Jean-Guy Berrin (jean-guy.berrin@inrae.fr)
INRAE https://orcid.org/0000-0001-7570-3745

Article

Keywords: Copper Radical Oxidases, Aliphatic Alcohols, Fungal Plant Pathogens, Haem-iron Peroxidase, Mutant Appressoria, Fungal Infection Machinery

Posted Date: May 27th, 2021

DOI: https://doi.org/10.21203/rs.3.rs-493001/v1

Unravelling the role of alcohol copper radical oxidases in fungal plant pathogens

Bastien Bissaro[1†], Sayo Kodama[2†], Hayat Hage[1], David Ribeaucourt[1,3,4], Mireille Haon[1], Sacha Grisel[1], A. Jalila Simaan[3], Fred Beisson[5], Stephanie M. Forget[6], Harry Brumer[6], Marie-Noëlle Rosso[1], Richard O´Connell[7], Mickaël Lafond[3], Yasuyuki Kubo[2*] and Jean-Guy Berrin[1*]

[1]INRAE, Aix Marseille Université, UMR1163 Biodiversité et Biotechnologie Fongiques, 13009, Marseille, France
[2] Faculty of Agriculture, Setsunan University, Osaka, Japan
[3] Aix Marseille Université, CNRS, Centrale Marseille, iSm2, Marseille, France
[4] V. Mane Fils, 620 route de Grasse, 06620 Le Bar sur Loup, France
[5]CEA, CNRS, Aix Marseille Université, Institut de Biosciences et Biotechnologies d'Aix-Marseille (UMR7265), CEA Cadarache, 13108 Saint-Paul-lez-Durance, France
[6] Michael Smith Laboratories, University of British Columbia, 2185 East Mall, Vancouver, BC, V6T 1Z4, Canada
[7] INRAE, UMR BIOGER, AgroParisTech, Université Paris-Saclay, Thiverval-Grignon, France

*Correspondence to: Yasuyuki Kubo (yasuyuki.kubo@setsunan.ac.jp) and Jean-Guy Berrin (jean-guy.berrin@inrae.fr)

[†]These authors contributed equally

Abstract

Copper radical oxidases (CRO) form a class of enzymes with a longstanding history encompassing diverse substrate specificities. While the biological function of most CROs remains unknown, we observed that CROs active on aliphatic alcohols are found only in fungal plant pathogens. Here, we unveil the role of these CROs and the identity of their natural redox partner, a haem-iron peroxidase. Combining multiscale approaches, we report that *Colletotrichum* and *Magnaporthe* appressoria (specialized cells that puncture the plant cuticles) co-secrete this pair of metalloenzymes early during penetration. We show *in vivo* that mutant appressoria lacking either or both enzymes have impaired penetration ability and pathogenicity. We reveal *in vitro* a finely-tuned enzyme interplay is responsible for the oxidation of plant cuticular long-chain alcohols into aldehyde products, suggested to act as key molecular signals in the fungal infection machinery. Our results open new avenues to design oxidase-specific inhibitors as anti-penetrants for crop protection.

Copper radical oxidases (CROs) are enzymes with diverse substrate specificities, and have been extensively studied since the late 1960s[1]. Today, CROs include galactose 6-oxidases (GalOx)[1], glyoxal oxidases[2], and broad specificity primary alcohol oxidases (AlcOx)[3,4]. Although glyoxal oxidases have been proposed to play a role in lignin degradation by fungal saprotrophs[2], the biological function of CROs is generally unknown despite decades of enzymological and structural research. During the course of our previous work[4], we noted that genes encoding secreted AlcOx orthologs are particularly widespread among phytopathogenic ascomycete fungi and absent in plants. Hence, given that long-chain primary alcohols are components of the waxy cuticle of aerial plant surfaces[5], we hypothesized that AlcOx could play a role in fungal pathogenesis.

Fungal phytopathogens represent a serious threat to plant health[6] and global food security[7]. *Magnaporthe* and *Colletotrichum* species rank among the top 10 most devastating fungal phytopathogens in the world and reduce crop yield by up to 30%[8]. Despite being separated by ca. 300 million years of evolution[9,10], these fungi share remarkable similarities in their infection strategy, notably the formation of a specialized cell dedicated to host penetration called an appressorium[11–13] (**Fig. 1a**). This dome-shaped, darkly melanized cell directs a high internal turgor onto a needle-like penetration peg[14–16], which emerges from a 2-500 nm pore at the appressorial base to puncture the plant's outer defensive barriers, the cuticle and epidermal cell wall. Despite major advances in our understanding of the cellular processes preceding[11,12,16–19] and following[20,21] plant cell entry, the (bio)chemical reactions occurring at this nanoscale plant-fungus interface and their role in host penetration remain poorly understood.

In this study, we used a combination of phylogenomics and fungal transcriptomics to unveil the pairing of AlcOx with a redox partner in two major fungal plant pathogens. We used mechanistic enzymology to validate and provide insights into the biochemical interplay between these metalloenzymes. Reverse genetics and live cell imaging allowed us to probe the *in vivo* function of the enzyme pair, thereby providing a holistic overview of this redox molecular mechanism operating in two distinct pathosystems of agricultural importance.

Results

Discovery of the tandem Perox-AlcOx

While studying the enzymology of *Colletotrichum* copper-radical AlcOx for biotechnological applications[4,22], we noticed the presence of a gene encoding a putative peroxidase located adjacent to an AlcOx-encoding gene (**Fig. 1b**). To strengthen this initial observation, we searched for *alcox* orthologs in 30 sequenced *Colletotrichum* genomes, which revealed the near-ubiquitous presence of a putative peroxidase (henceforth called "Tandem Peroxidase") in a head-to-head arrangement with each AlcOx-encoding gene (**Extended Data Fig. 1**). Moreover, these Tandem Peroxidases are never found in combination with other types of CROs (**Extended Data Fig. 1c**) and both proteins encoded by the *perox-alcox* pair are predicted to be secreted (**Supplementary Table 1**). These observations aroused our interest because it is known that CROs require activation by horseradish peroxidase (HRP) for maximum activity *in vitro*[23,24].

Our phylogenetic analysis of the peroxidase-catalase superfamily showed that the Tandem Peroxidases cluster together in a sister clade within the under-explored ascomycete

Class II peroxidases[25] (**Extended Data Fig. 2a**). Furthermore, Tandem Peroxidases form a distinct clade amongst the 333 Class II peroxidases found in *Colletotrichum* species (**Extended Data Fig. 2b**), suggestive of neofunctionalization. More broadly, a search for the co-occurrence of *perox* and *alcox* orthologs across fungal genomes revealed that the pair is also encoded by *Magnaporthe* species, including the infamous causal agent of rice blast, *Magnaporthe oryzae* (syn. *Pyricularia oryzae*) (**Supplementary Table 2).** Mapping the occurrence of Perox-AlcOx protein pairs and their corresponding genomic neighborhoods onto a phylogeny of representative pathogenic ascomycetes (**Fig. 1b**, **Extended Data Fig. 3**) allowed us to conclude that: (i) the pair is present in *Magnaporthe spp.* and most *Colletotrichum* species complexes, and has disappeared in the most recently evolved *Colletotrichum acutatum* species complex; (ii) the genomic environment of the pair is not conserved between the species complexes while the head-to-head organization is, indicating a selection pressure and critical role for the pair; (iii) the formation of melanized appressoria/hyphopodia does not strictly correlate with the presence of the pair (**Fig. 1b**).

To provide further evidence for the functional linkage of both the *perox* and *alcox* gene products, we parsed transcriptomic data available for the fungal species harboring this pair. Remarkably, this analysis revealed that both genes are always tightly co-expressed at the appressorium stage in various pathosystems involving *Colletotrichum* species attacking maize, fruits, and model plants[26,27], and *M. oryzae* attacking rice and barley[28,29] (**Fig. 1c,d**). Notably, expression remains relatively low and occurs within a narrow time window, which may explain why these genes have been overlooked in previous studies. Despite discrepancies in experimental design underlying the publicly available transcriptomics datasets, the fact that a similar conclusion is reached for the different pathosystems provides a high level of confidence in this observation.

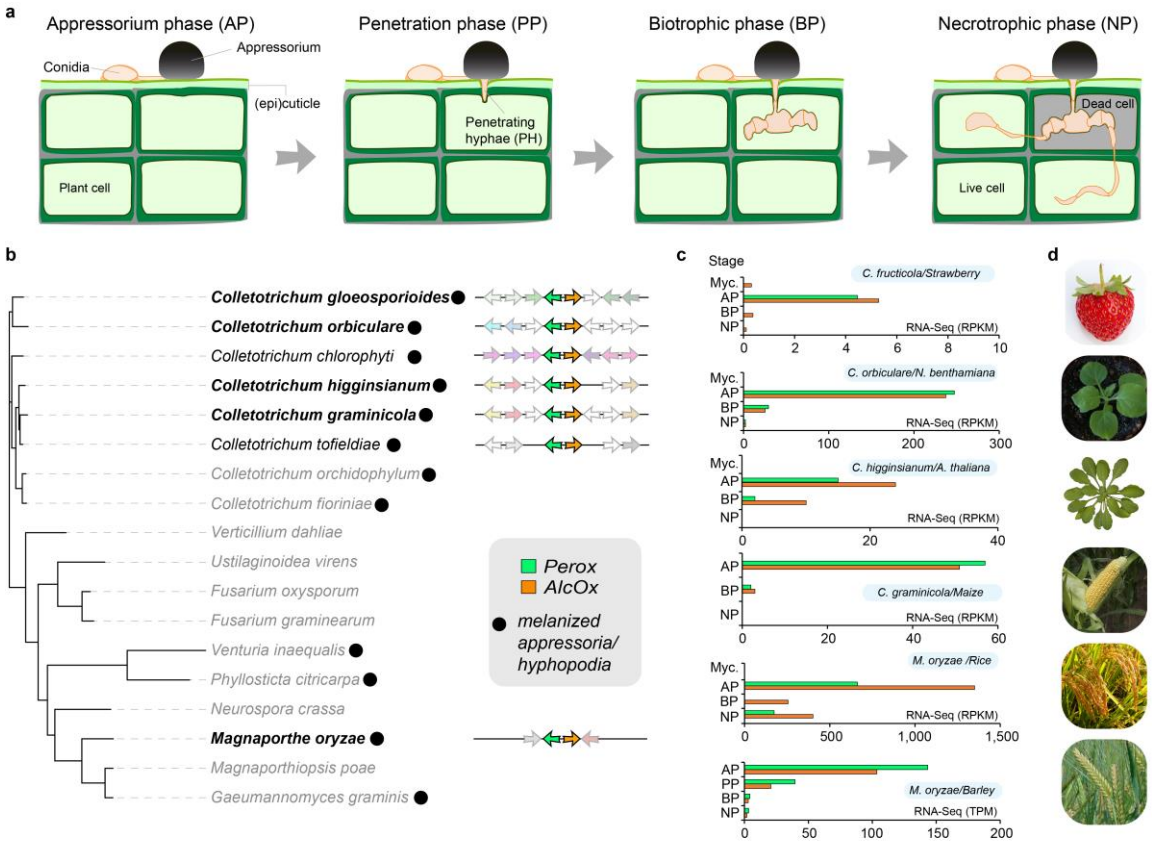

Fig. 1 | Genomic and transcriptomic analysis of the Perox-AlcOx pair. a, The multistage plant infection process of appressorium-forming fungi: appressorium (AP), penetration (PP), biotrophic (BP) and necrotrophic (NP) phases. **b**, Phylogenomic occurrence of the *perox-alcox* pair and consensus genomic environment amongst pathogenic ascomycetes (black bold lettering indicates species for which we show transcriptomics data (panel c) and grey lettering indicates absence of the gene pair). Selected *Colletotrichum* species and associated consensus sequences are representative of the species complex they belong to (note that *C. fructicola* shown in panel c belongs to the *C. gloeosporioides* species complex; see **Extended Data Fig. 3**). **c**, Time-course transcriptomic analysis of the Tandem Peroxidases (Perox, green) and AlcOx (orange) encoding genes (see gene numbers in **Supplementary Table 1**) during plant infection for different pathosystems (Myc., Mycelium)[26–29]. Actual time points associated with the different infection stages are provided in the material and methods section. **d**, Illustration of targeted hosts.

Tandem Perox-AlcOx oxidize plant long chain alcohols

As a prelude to analyzing their biological function *in vivo*, we studied the substrate specificity and enzyme interplay of the Perox-AlcOx pair *in vitro* (**Fig. 2a**). *C. orbiculare* was selected as a model because it causes the economically important anthracnose disease of cucurbits (e.g., melons, cucumber). Despite the notorious difficulties associated with such metalloenzymes, we successfully produced in the yeast *Pichia pastoris* the recombinant copper-radical AlcOx and haem-iron tandem peroxidase from *C. orbiculare* (hereafter *Cor*AlcOx and *Cor*Perox, respectively). In keeping with its close phylogenetic relationship with AlcOx orthologs from *C. graminicola* and *C. gloeosporioides*[4] (**Extended Data Fig. 1a**), *Cor*AlcOx oxidized both aromatic and long-chain aliphatic primary alcohols (**Extended Data Fig. 4a**). The latter are native substrates present in the cuticle of many plant species[5] including cucumber (*vide infra*).

On the other hand, *Cor*Perox was confirmed to be a peroxidase, albeit with moderate catalytic efficiency (k_{cat} = 1.52 ± 0.02 s^{-1}, K_M^{H2O2} = 80 ± 3 µM, k_{cat}/K_M = 1.9 × 10^4 ± 0.1 $s^{-1}.M^{-1}$) compared to the only previously characterized ascomycete Class II peroxidase[25], commercial horseradish peroxidase (HRP)[30], and well-studied basidiomycete lignin-active peroxidases[31] (k_{cat}/K_M = 10^4-10^7 $s^{-1}.M^{-1}$). *Cor*Perox was only active on low redox-potential substrates and not on any canonical lignin-active peroxidase substrates (**Extended Data Fig. 4b**), and required the presence of calcium ions for stability (**Extended Data Fig. 4c**). These observations are in agreement with structural predictions (**Extended Data Fig. 5**), which indicate the presence of two conserved calcium ion binding sites, but absence of the manganese binding site and the tryptophan involved in long-range electron transfer, two key features of lignin-active peroxidases[32].

Despite its comparatively low peroxidase activity, *Cor*Perox activates *Cor*AlcOx for oxidation of primary alcohols in a dose-dependent manner, and to a much greater extent than the plant peroxidase HRP does (**Fig. 2b**). Curiously, the pH optima of *Cor*AlcOx and *Cor*Perox were markedly different (ca. 8 and 4, respectively, **Extended Data Fig. 4d**). Taken together, these results indicate that AlcOx activation is not dependent on highly efficient peroxidase activity. We also heterologously produced the Perox-AlcOx pair from the rice blast pathogen *M. oryzae*, of which *Mor*AlcOx was recently confirmed to be a primary alcohol oxidase[33]. Here, we obtained an activation profile for the *Mor*Perox-*Mor*AlcOx resembling that observed for the *C. orbiculare* pair (**Extended Data Fig. 4e** *cf.* **Fig. 2b**).

We used electron paramagnetic resonance (EPR) spectroscopy to obtain a deeper understanding of the activation of AlcOx by the Tandem Peroxidase (**Fig. 2c**). Reduction in the EPR signal of the *inactive* Cu(II)-non-radical form of *Cor*AlcOx upon addition of *Cor*Perox was supportive of one-electron oxidation leading to the EPR silent, *active* Cu(II)-radical form (**Fig. 2a,c**). This change in electronic structure, observed in the absence of any substrate, confirms the activity-independent activating role of *Cor*Perox. It also indicates a close contact between the enzymes during the activation process, and is concordant with the sigmoidal, titration-like curves observed during activity assays carried out in the presence of substrate (**Fig. 2b**).

Having determined optimal enzyme activation conditions, we then probed further the activity of the *Cor*Perox-*Cor*AlcOx pair on biologically relevant aliphatic alcohols. Despite challenges associated with substrate solubility in aqueous buffer, we clearly detected activity

on hexadecan-1,16-diol and octadecanol, as well as on a crude preparation of waxes extracted from cucumber cotyledons (**Fig. 2d**). Importantly, such activity was detected only when both enzymes were present. Product analysis by gas chromatography unambiguously indicated that octadecanol was oxidized to the corresponding aldehyde (**Extended Data Fig. 4f**). Interestingly, the binding surfaces of AlcOx orthologs are considerably more hydrophobic than that of GalOx (**Fig. 2e,f**), which suggests that AlcOx evolved to interact with the hydrophobic plant cuticle.

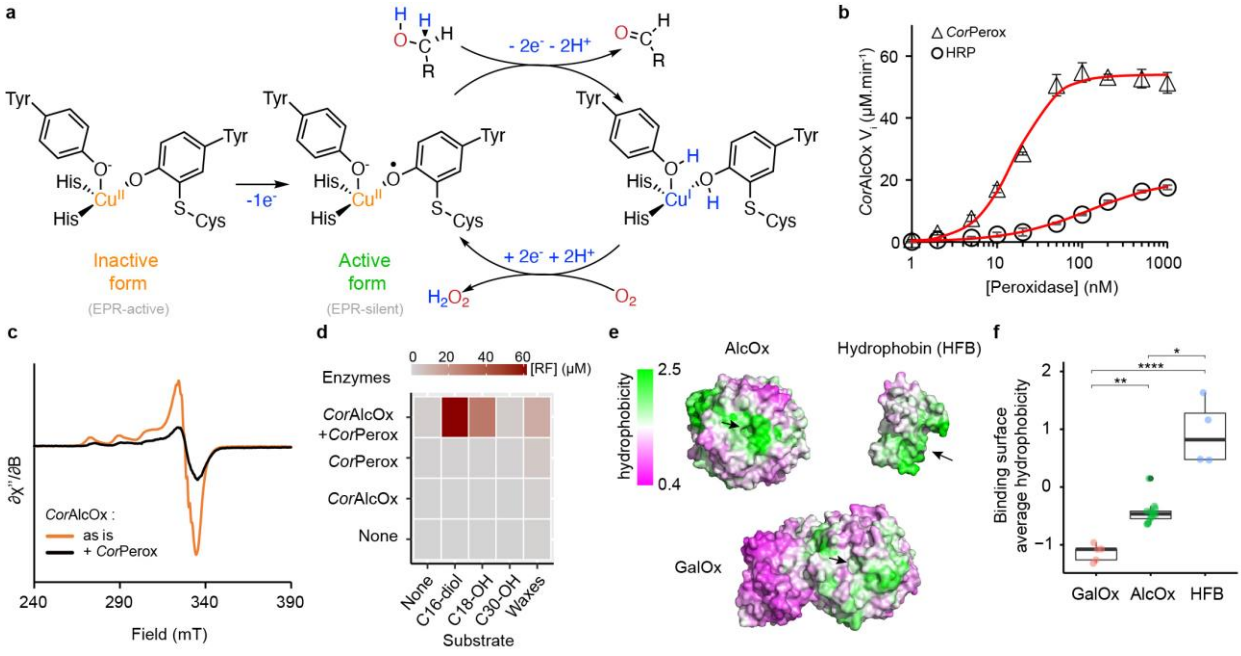

Fig. 2 | Biochemical and biophysical evidence for the interplay between *Cor*Perox and *Cor*AlcOx. **a**, Reaction mechanism of CROs showing activation of the resting, inactive form of the enzyme via formation of a tyrosine radical, yielding the Cu(II)-radical active form. The latter will oxidize an alcohol into the corresponding aldehyde followed by regeneration of the active form via the two-electron reduction of O_2 into H_2O_2. **b**, *Cor*AlcOx oxidation rate in presence of varying amounts of HRP or *Cor*Perox. **c**, EPR spectra of inactive *Cor*AlcOx before (orange curve) and after mixture with *Cor*Perox (black curve). EPR parameters of the Cu(II) inactive form: $g_z = 2.270$, $A_z^{Cu} = 171\ 10^{-4}\ cm^{-1}$, $g_x = 2.047$, $A_x^{Cu} < 50\ 10^{-4}\ cm^{-1}$, $g_y = 2.054$, $A_y^{Cu} < 50\ 10^{-4}\ cm^{-1}$ and super-hyperfine coupling constant corresponding to two N-ligands $A^N = 43\ 10^{-4}\ cm^{-1}$. **d**, Activity of *Cor*Perox-*Cor*AlcOx on crude extract of cucumber waxes and derived long chain aliphatic alcohols, monitored via the production of chromogenic resorufin (RF), product of the Perox-catalyzed oxidation of Amplex-Red by H_2O_2, the latter being the co-product of AlcOx-catalyzed oxidation of primary alcohols into aldehydes. **e,f**, Surface hydrophobicity (**e**) and average hydrophobicity (expressed as the grand average of hydropathy (GRAVY) score) (**f**) of the binding surface (indicated with black arrow) of GalOx (PDB 1GOG)[34], AlcOx (PDB 5C92)[4] and hydrophobin (HFB, PDB 2N4O)[35]. **P*<0.05, ***P*<0.01, *****P*<0.0001, Kruskal-Wallis test.

The Perox-AlcOx pair gates plant penetration

To investigate the role of the Perox-AlcOx pair in plant infection, we isolated single and double gene deletion mutants of *C. orbiculare* and *M. oryzae* (**Extended Data Fig. 6**). Inoculation of conidial suspensions onto intact cucumber cotyledons for *C. orbiculare*, or barley leaves for *M. oryzae*, showed that fewer and smaller lesions were formed compared to the wild-type strains (**Fig. 3a-d**). For instance, the proportion of lesions > 4 mm fell from 95 % to < 20% for *C. orbiculare* on cucumber. Furthermore, similar phenotypes were obtained for single and double mutants, suggesting that both oxidases are crucial, in both pathosystems.

Focusing on *C. orbiculare* as a model system, neither single nor double *perox*/*alcox* deletion mutants were affected in mycelial growth (**Extended Data Fig. 6a**). Microscopy revealed that the significant loss of pathogenicity is due to a large decrease in the frequency of host penetration by mutant appressoria (**Fig. 3e**). However, morphogenesis, cell wall melanization, and turgor build-up within appressoria cells were virtually indistinguishable from those of the wild type strain (**Extended Data Fig. 6, b-e**). The next step in the infection process is the emergence of a needle-like penetration peg through a pore in the basal cell wall of the appressorium (**Fig. 1a**), during which actin assembly at the pore provides rigidity[36]. Using a red fluorescent protein/actin-binding protein fusion (Lifeact-RFP), we found normal actin assembly at the appressorium pore for both the single and double mutants inoculated onto cucumber cotyledons (**Extended Data Fig. 6f,g**).

Remarkably, mutants could penetrate and form hyphae inside inert cellophane membranes (**Extended Data Fig. 7a-c**) and caused wild-type-like lesions when inoculated on mechanically *wounded* cucumber cotyledons (**Extended Data Fig. 7d,e**), in contrast to the crippled invasive capacity observed on intact leaves (**Fig. 3e**). This points to a mechanism involving plant surface compounds, concordant with the catalytic activity of the Perox-AlcOx pair (**Fig. 2**). These results collectively indicate that *Cor*AlcOx and *Cor*Perox play a crucial role during the early penetration stage, but are not involved in either appressorium or peg formation.

To further examine the function of the Perox-AlcOx pair during plant infection, we attempted to localize the proteins by live-cell imaging of *Cor*AlcOx-mCherry and *Cor*Perox-GFP driven by their native promoters. Although the *Cor*AlcOx-mCherry and *Cor*Perox-GFP complemented the defect in pathogenicity of the deletion mutants, fluorescence of *Cor*AlcOx-mCherry and *Cor*Perox-GFP was not detectable during appressorium formation on cucumber cotyledons (**Extended Data Fig. 8a**), suggesting that gene expression was too low, consistent with transcriptomic data (**Fig. 1c**), or that the gene products were secreted and diffused away from the penetration site. However, the constitutive overexpression of *Cor*AlcOx-mCherry and *Cor*Perox-GFP, driven by the *translation elongation factor (TEF)* promoter, revealed that both proteins accumulate specifically at the appressorial penetration pore and that signal intensity increased during penetration peg formation (**Fig. 3f**, **Extended Data Fig. 8b,c,** and **Supplementary Movie 1**). This protein co-localization observed *in vivo* is consistent with gene co-expression data (**Fig. 1c**) and rationalizes the co-operative activity demonstrated by biochemical assays (**Fig. 2**). Remarkably, *Cor*AlcOx-mCherry and *Cor*Perox-GFP were detected at the plant surface beneath detached appressorium, at the penetration pore (**Fig. 3g**), suggesting that the tandem metalloenzymes are secreted from appressoria into the plant epidermis. Strikingly, *Cor*AlcOx-mCherry and *Cor*Perox-GFP were not detected at the

penetration site on cellophane membranes (**Extended Data Fig. 8d**), suggesting that interaction of the fungus with the plant surface triggers local recruitment of the tandem metalloenzymes to the pore.

To explore further the role of Perox-AlcOx in pathogenicity, we exposed the *C. orbiculare* single and double mutants to a product of the AlcOx, *viz.* the aliphatic long chain aldehyde *n*-octadecanal. For all gene deletion mutants, the addition of *n*-octadecanal partially restored appressorium penetration ability and lesion formation on cucumber leaves (**Extended Data Fig. 9a-c**). Furthermore, on heat-shocked cotyledons, in which plant defenses are attenuated, the pathogenicity of *C. orbiculare* mutants remained lower than the wild-type (**Extended Data Fig. 9d**), suggesting that the Perox-AlcOx pair is not involved in overcoming plant defenses. In support of this, we found that appressoria of the mutants induced the formation of plant callose deposits (a pre-invasive defense response) with the same frequency as wild-type appressoria (**Extended Data Fig. 9e,f**).

To probe the presence of potential natural substrates of the fungal AlcOx in the neighborhood of the penetration site, we carried out a compositional analysis of waxes present at the surface of cucumber cotyledons (**Extended Data Fig. 10**). This analysis showed that the extracted waxes are mainly composed of odd-numbered alkanes (C27-C33) and even-numbered long-chain primary alcohols (C24-C32). Fatty aldehydes were not found in quantifiable amounts (only traces). Thus, this experiment demonstrates that AlcOx substrates are present at the plant surface while AlcOx reaction products are not. Taken together, our results suggest that the role of the fungal Perox-AlcOx pair is to generate long chain aldehydes (e.g., C18 and longer) that may function as signal molecules required to prime the fungus for efficient plant infection.

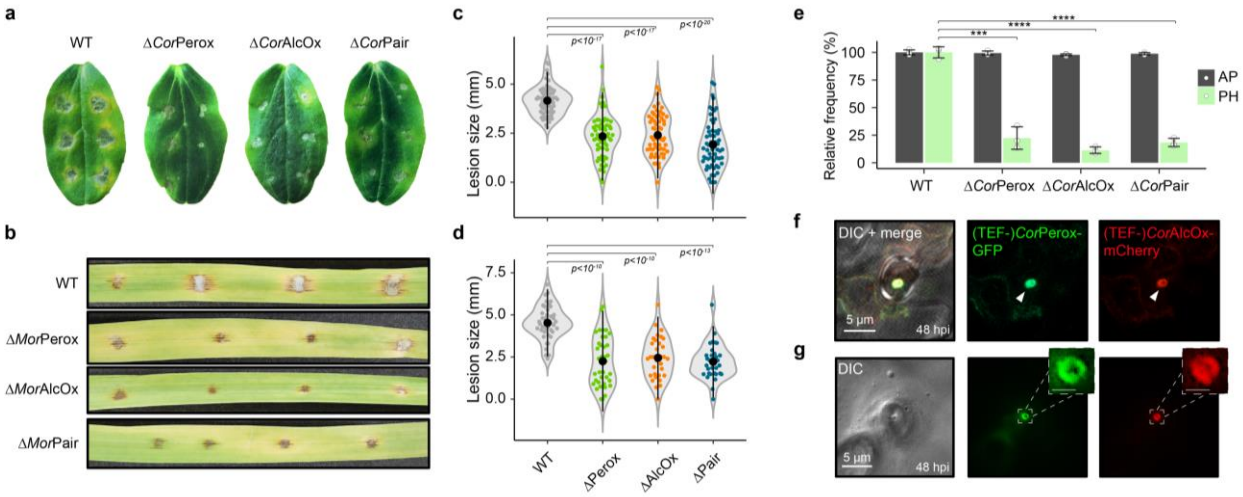

Fig. 3 | *In vivo* characterization of the role of the Perox-AlcOx pair during plant infection. a-d, Infection phenotypes (**a,b**) and violin plot of the necrotic lesions size (**c,d**), at 5 dpi, for the wild-type (WT) and *perox/alcox* deletion mutants of *C. orbiculare* on intact cucumber (*Cucumis sativus*) cotyledons (**a,c**) and of *M. oryzae* on barley (*Hordeum vulgare*) (**b,d**). For each strain/plant combination, at least 60 inoculations were carried out. **e**, Relative frequency (WT set to 100%) of development of normal appressorium (AP) and penetrating hyphae (PH) by *C. orbiculare* strains on cucumber cotyledons. Data are presented as average values (>300 appressoria for each replicate, n = 3 independent biological replicates) and error bars show s.d.. **f,g**, Localization of *C. orbiculare* tandem oxidases on cotyledons at 48 hpi, in the presence of appressoria cells (**f**) or after detachment of the appressoria from the surface leaf (**g**). In panel **f**, white arrowheads indicate enzyme accumulation at the appressorium pore. In panel **g**, enlarged insets show a ring-like localization of the enzymes (scale bar = 1 µm). In panels **c-e**, a one-tailed independent *t*-test for each mutant *vs* WT was applied (****P*<0.001, *****P*<0.0001).

Discussion

Research on plant invasion by appressorium-forming fungi teaches us that the development of the specialized infection structures is an extremely complex, finely regulated process. In this study, we have shown that fungal AlcOx have a very different biological function than the few distantly-related CROs for which roles in morphogenesis[37,38] or lignin degradation[2] were proposed.

Analogy with some plant cell wall-active metalloenzymes and lignin-active peroxidases[31] would imply a direct role of these metalloenzymes in disrupting the cuticular barrier structure. However, our results rather suggest that the oxidative action of Perox-AlcOx on very-long chain (VLC) alcohols generates signaling molecules functioning in a yet-to-be-elucidated biochemical cascade. It is well-known that exogenous addition of VLC alcohols/aldehydes induces conidia to differentiate into appressoria cells[18,39]. However, the specific deployment of the tandem metalloenzymes at the later appressorium stage, together with the fact that the *perox-alcox* mutants form normal, pressurized appressoria, and retain penetration ability on cellophane, indicates that the cuticle-derived compounds generated by the enzyme pair do not act as inducers of appressorium/peg morphogenesis[40]. Nonetheless, the mutants were defective in puncturing intact plant cuticles, suggesting that cuticular alcohol oxidation provides a chemical cue required for plant cell entry, consistent with the partial restoration of pathogenicity of *perox-alcox* mutants upon addition of the enzyme product *n*-octadecanal.

The fact that *perox-alcox* mutants retained a residual ability to penetrate the plant cells indicates there is not an absolute requirement for this pair of metalloenzymes. Several hypotheses can be formulated to explain this observation: (i) the fungus possesses compensatory mechanisms that remain to be uncovered; (ii) the fungus invades the plant through micro-injuries; (iii) trace aldehydes present in the cucumber leaves could be sufficient to allow some rare penetration events. It is noteworthy that aliphatic aldehydes are prone to O_2-mediated oxidation and that their natural content and spatial distribution/orientation varies between plants, leaf developmental stages, or even between infection sites on a same leaf. Taking this into account, it is a possibility that a favorable balance between aldehydes and inhibitors found in waxes is necessary to trigger infection, and such balance may vary from one pathosystem to the other. Thus, we speculate that the acquisition of the Perox-AlcOx pair provides the ecologically widespread *Colletotrichum* and *Magnaporthe* species with an advantage, namely an *in-house* "locksmith" (i.e., the tandem metalloenzymes) ensuring production of the entry key (i.e., the aldehyde) needed to enter into the next pathogenesis stage (penetration). This hypothesis remains to be fully demonstrated.

It is interesting to speculate why Nature has evolved such a complex enzymatic system relying on haem-iron peroxidase and elaborate copper radical chemistry when simpler, mono-enzyme systems could be employed for the same purpose (e.g. VLC alcohols FAD-dependent oxidases[41]). We show that the functional integrity of the secreted tandem metalloenzymes system endows pathogenic fungi with fine control over oxidation reactions in the extracellular space. We propose that the copper-radical center equips CROs with a "redox switch" to turn on activity with high spatio-temporal resolution, when paired with a cognate peroxidase (**Fig. 4**). More generally, our study suggests that fungi have evolved ways of controlling important reactions that are seemingly out of reach, i.e. beyond the bounds of the fungal plasma

membrane and cell wall, through tight genetic regulation and protein interplay between secreted oxidoreductases.

In conclusion, using a combination of *in silico*, *in vitro* and *in vivo* approaches, we have unveiled the biological function of AlcOx-type CRO and its natural redox partner acting as secreted virulence factors during early infection in two distinct pathosystems (**Fig. 4**). The specific occurrence of the Perox-AlcOx pair in most *Colletotrichum* and *Magnaporthe* species raises the possibility that functionally equivalent, coupled oxidative enzymatic mechanisms may operate in other appressorium-forming fungal pathogens. It is noteworthy that the enzymology-driven approach pursued here was essential to bring to light this unique mechanism, because low expression levels, fine temporal tuning, and highly localized co-secretion of the Perox-AlcOx would have evaded classical 'omic approaches. We anticipate that the present discovery will open new avenues of fundamental and applied research, including the development of oxidase-specific inhibitors as surface-acting, anti-penetrant drugs for crop protection.

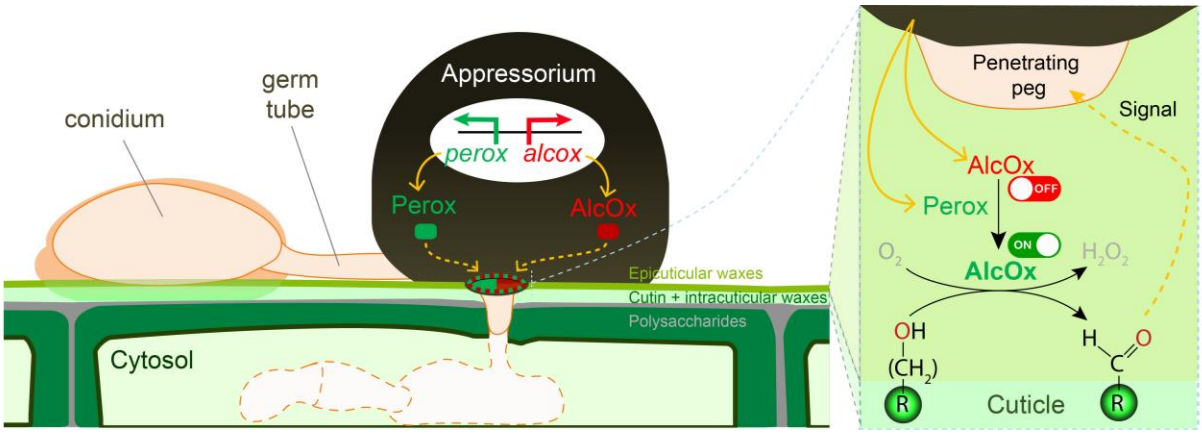

Fig. 4 | Schematic summary of the recruitment of the fungal Perox-AlcOx pair during early plant penetration. The right-hand panel illustrates the Perox-AlcOx reaction occurring at the fungus-plant interface.

Methods

Chemicals and commercial enzymes

Most chemicals were purchased from (Darmstadt, Germany) or VWR (Fontenay-sous-Bois, France) unless stated otherwise. Molar concentrations of type II HRP (Sigma-Aldrich; MW 33.89 kDa) were estimated by Bradford assay. *n*-Octadecanal was purchased from TCI-Europe (Zwijndrecht, Belgium). All alcohol substrates stock solutions were prepared either in H_2O or in acetone and stored at -20°C. The concentration of H_2O_2 stock solution was verified at 240 nm ($\varepsilon^{240} = 43.6\ M^{-1}.cm^{-1}$).

Bioinformatics

Species tree of the 18 ascomycete genomes (shown in **Fig. 1b**) was constructed as previously described[42]. Core clusters containing only one protein-coding gene per species were identified using FastOrtho[43] with the following parameters: 50% identity and 50% coverage. Each cluster was aligned with MAFFT 7.221[44], and curated alignments were concatenated with Gblocks 0.91b[45]. The tree was finally constructed with RAxML 7.7.2[46] (PROTGAMMAWAG model and 500 bootstrap). Phylogenetic analysis of AA5_2 genes and «standard» haem peroxidases (PFAM 00141, including Class II peroxidases) from 30 *Colletotrichum* genomes relied on 72 and 333 sequences, respectively (see **Extended Data Fig. 2** legend and **Supplementary Table 3** for more details). The phylogenetic analysis of the peroxidase-catalase superfamily relied on 150 sequences encompassing Class I (intracellular peroxidases), II (fungal secreted peroxidases) and III (plant secreted peroxidases) peroxidases and from so-called Hybrid B peroxidases, as previously reported[47]. Subsequently to manual curation (removing signal peptides), the sequences were first aligned using MAFFT-DASH (L-INS-i method)[48] and the resulting multiple sequence alignment (MSA) was used to infer a phylogenetic tree using RAxML (1000 bootstraps). The trees were then visualized in iTOL[49] and edited in Illustrator®.

For the gene neighborhood survey, we retrieved 4 genes located upstream and downstream of each *Colletotrichum*'s AA5_2 query (72 sequences). The resulting 569 genes were assigned to 78 different PFAM domains. The frequency of occurrence of a given type of domain in the neighborhood of each AA5_2 phylogenetic clade was then computed and visualized in Excel.

For interrogating the co-occurrence of both Perox and AlcOx-coding genes beyond *Colletotrichum* species two independent BLAST searches were run against the NCBI non-redundant database, using *Cor*AlcOx and *Cor*Perox as query sequences. 1,000 AlcOx-like (down to 37% sequence identity) and 1,000 Perox-like (25% sequence identity) sequences along with their corresponding source microorganism were retrieved. A cross-comparison of both lists of microorganisms, applying different sequence identity-based thresholds (60% for AlcOx and 30% for Perox) returned the list of species harboring both type of enzymes.

Structural homology models were generated with Phyre 2.0[50]. Surface hydrophobicity of selected CROs was computed with the "protein-sol patches" online software[51]. Average hydrophobicity of the binding surface was determined as follows: using PyMOL 2.4, we selected the residues constituting the entire binding surface of *Fgr*GalOx, *Cgr*AlcOx and equivalent residues (based on MSA) in orthologous enzymes (5 GalOx and 11 AlcOx in total)

as well as those of 4 characterized hydrophobins (PDB 2N4O, 2LSH, 1R2M and 2FZ6) as hydrophobic protein reference. Average hydrophobicity of the selected residues was computed as a GRAVY index score (Kyte-Doolittle method)[52].

Transcriptomics data were retrieved from publicly available datasets[26–29]. To normalize different dataset longitudinally, we expressed reported sampling time points as infection stages in Fig. 1 as follows (hpi = hours post-infection): for *C. fructicola nara gc5/strawberry*[27], AP (24 hpi), BP (72 hpi) and NP (144 hpi); for *C. orbiculare/N. benthamiana*[27], AP (24 hpi), BP (72 hpi) and NP (168 hpi); for *C. higginsianum/A. thaliana*[26], AP (22 hpi), BP (40 hpi) and NP (60 hpi); *C. graminicola/Maize*[26], AP (22 hpi), BP (40 hpi) and NP (60 hpi); *M. oryzae/Rice*[28], AP (8 hpi), BP (24 hpi) and NP (48 hpi); *M. oryzae/Barley*[29], AP (12 hpi), PP (24 hpi), BP (36 hpi) and NP (48 hpi).

DNA Cloning and strain production

DNA cloning and strain production of the AA5_2 alcohol oxidases (AlcOx) from *Colletotrichum graminearum* (*Cgr*AlcOx, Genbank ID XM_008096275.1, Uniprot ID E3QHV8) was already carried out in previous study[4]. The intron-free sequences of the genes coding for the AlcOx from *Colletotrichum orbiculare* MAFF 240422 (*Cor*AlcOx, Genbank ID TDZ17043.1, Uniprot ID N4UTF2), the AlcOx from *Magnaporthe oryzae* (*Mor*AlcOx, Genbank ID XM_003719321.1, Uniprot ID G4NG45), the Tandem Peroxidase (Perox) from *Colletotrichum orbiculare* (*Cor*Perox, Genbank ID TDZ17044.1, Uniprot ID N4UUY4) and the Tandem Peroxidase from *Magnaporthe oryzae* (*Mor*Perox, Genbank ID XM_003719322.1, Uniprot ID G4NG46) were synthesized after codon optimization for expression in *P. pastoris* and inserted into a modified pPICZαC vector using *Xho*I* and *Not*I restriction sites in frame with the α secretion factor at N-terminus (i.e. without native signal peptide) and with a $(His)_6$-tag at the C-terminus (without *c*-myc epitope) (Genewiz, Leipzig, Germany). Transformation of competent *P. pastoris* X33, selection of zeocin-resistant *P. pastoris* transformants screened for protein production was carried out as described by Haon et al.[53]. The best-producing transformants were conserved as glycerol stock at – 80°C.

Heterologous protein production in flasks

All proteins were first produced in 2 L Erlenmeyer flasks. To this end, single colonies of *P. pastoris* X33 expressing each gene of interest were individually streaked on a YPD agar plate containing Zeocin (100 $\mu g.mL^{-1}$) and incubated 3 days at 30°C. A single colony was then used to inoculate 5 mL of YPD, in a 50 mL sterile Falcon tube and incubated during 5 h (30°C, 160 rpm). This pre-culture was used to inoculate at 0.2% (vol/vol) 500 mL of BMGY medium, in a 2 L Erlenmeyer flask, incubated during approximately 16 h (30°C, 200 rpm) until the $OD_{600\ nm}$ reached 4−6. The produced cellular biomass was then harvested by centrifugation (5 min, 16°C, 3,000 x *g*). For the AlcOx, the cell pellet was then resuspended in 100 mL BMMY medium supplemented with methanol (1%, vol/vol) and $CuSO_4$ (500 µM). The culture was incubated for 3 days (16°C, 200 rpm), with daily additions of methanol (1% added, vol/vol). The Tandem Peroxidases production conditions were optimized and varied from the standard protocol as follows: the BMMY was supplemented with methanol (3% vol/vol), hemin (25 µM) and $CaCl_2$ (2 mM). The culture was incubated for 3 days (20°C, 200 rpm), with daily additions of methanol (3%, vol/vol) and hemin (25 µM).

Then, the extracellular medium was recovered by centrifugation (10 min, 4°C, 3,000 x *g*) and the supernatant filtrated on 0.45 µm membrane (Millipore, Massachusetts, USA) and stored at 4°C prior to purification.

Heterologous protein production in bioreactors

The upscaled production of *Cor*Perox was carried out in 1.3 L and 7.5 L bioreactors (New Brunswick BioFlo 115 fermentor, Eppendorf, Germany) as per the *P. pastoris* fermentation process guidelines (Invitrogen) with the following optimizations: the glycerol fed-batch phase was replaced by a sorbitol and methanol transition phase, besides 200 µM (1.3 L bioreactor) and 150 µM (7.5 L bioreactor) of hemin were added to the methanol solution. $CaCl_2$ (10 mM final) was added to the crude protein solution before being either directly purified or flash-frozen in liquid nitrogen and stored at -80°C. We verified that flash-freezing did not cause any activity loss, for both AlcOx and Perox enzymes.

Protein purification

The filtered *Cor*AlcOx and *Mor*AlcOx crude supernatants were adjusted to pH 8.5, filtered on 0.22 µm filters (Millipore, Molsheim, France), and purified by anion exchange chromatography (DEAE) on a HiPrep FF 16/10 column (GE Healthcare, USA). Elution was performed by applying a linear gradient from 0 to 500 mM NaCl (in Tris-HCl buffer 50mM, pH 8.5) over 20 column volumes, with a flow rate set to 5 $mL.min^{-1}$.

The filtered *Cor*Perox and *Mor*Perox culture supernatant was adjusted to pH 7.8 just before purification and filtered on 0.22 µm filters (Millipore, Molsheim, France). Depending on the volume to purify, the crude protein sample was either loaded on a His-Trap HP 5-mL column (GE Healthcare, Buc, France) on a HisPrep FF 16/10 column (GE Healthcare) connected to an ÄKTAxpress system (GE Healthcare) equilibrated with HEPES (10 mM, pH 8.0), NaCl (100 mM), $CaCl_2$ (2 mM) and imidazole (10 mM) buffer. Each $(His)_6$-tagged recombinant enzyme was eluted with HEPES (10 mM, pH 8.0), NaCl (100 mM), $CaCl_2$ (2 mM) and imidazole (500 mM) buffer. The Tandem Peroxidases were further purified by size exclusion chromatography, using a HiLoad 26/600 Superdex 200 pg column (GE Healthcare) operated at 2.5 mL/min and with a running buffer containing HEPES (10 mM, pH 8.0), NaCl (100 mM) and $CaCl_2$ (2 mM).

After SDS-PAGE analysis, fractions containing the recombinant enzyme were pooled, concentrated and buffer exchanged in sodium phosphate (50 mM, pH 7.0) for the AlcOx or in HEPES (10 mM, pH 8.0), NaCl (100 mM) and $CaCl_2$ (2 mM) buffer for the Tandem Peroxidases.

Protein concentrations of *Cgr*AlcOx (52,337 Da, ε^{280} = 101,215 $M^{-1}.cm^{-1}$), *Cor*AlcOx (52,317 Da, ε^{280} = 92,735 $M^{-1}.cm^{-1}$), *Mor*AlcOx (62,894 Da, ε^{280} = 90,020 $M^{-1}.cm^{-1}$), *Cor*Perox (26,137 Da, ε^{280} = 21,345 $M^{-1}.cm^{-1}$), and *Mor*Perox (26,290 Da, ε^{280} = 24,450 $M^{-1}.cm^{-1}$) were determined by the Bradford assay[54] using BSA as reference protein as well as by UV absorption at 280 nm using a Nanodrop ND-200 spectrophotometer (Thermo Fisher Scientific, Massachusetts, USA).

Enzyme assays

For screening the substrate specificity of CRO-AlcOx enzymes, the alcohol substrates were prepared in sodium phosphate buffer (50 mM, pH 7.0) in 96-well microplates and reactions

were initiated by the addition of a pre-mix of CRO-AlcOx (1 nM final concentration), HRP (0.1 $mg.mL^{-1}$) and 2,2′-azino-bis(3-ethylbenzothiazoline-6-sulfonic acid (ABTS, 500 μM) in sodium phosphate buffer (50 mM, pH 7.0). The tested substrates included D-glucose (50 mM final concentration, D-Glc), D-galactose (50 mM, D-Gal), D-raffinose (50 mM, D-Raf), xyloglucan (0.1% mM, XG), butan-1-ol (3 mM), butan-2-ol (3 mM), octan-1-ol (3 mM), decan-1-ol (3 mM), 2,4-hexadiene-1-ol (3 mM, HD-OH), glycol aldehyde dimer (3 mM, GAD), benzyl alcohol (3 mM, BnOH), 4-hydroxybenzyl alcohol (3 mM, p-OH BnOH), vanillic alcohol (3 mM, Van-OH), syringic alcohol (3 mM, Syr-OH) and cinnamyl alcohol (3 mM, Cin-OH). The absorbance of the final reaction (100 μL total volume) was monitored at 414 nm using a microplate spectrophotometer (TECAN), thermostated at 23°C. The 414 nm absorbance allows to determine the concentration of ABTS cation radical over time ($ABTS^{\bullet+}$, ε^{414} = 31,100 $M^{-1}.cm^{-1}$), and in turn the rate of alcohol oxidation, considering a peroxidase reaction stoichiometry for (H_2O_2:$ABTS^{\bullet+}$) of 1:2 and a CRO-AlcOx reaction stoichiometry for (alcohol:H_2O_2) of 1:1.

For screening the substrate specificity of *Cor*Perox, unless stated otherwise the enzyme (0.125 μM final) was prepared in citrate-phosphate buffer (50 mM, pH 4.0 to 7.0) in 96-well microplates (for wavelength in the visible range) or in 1 mL Quartz cuvettes (for UV range), in the presence of various substrates (*vide infra*). Reactions were initiated by the addition of H_2O_2 (100 μM final), incubated at 23°C, and monitored spectrophotometrically at the wavelengths indicated below. The tested peroxidase substrates included: ABTS (500 μM) converted into $ABTS^{\bullet+}$ (ε^{414} = 31,100 $M^{-1}.cm^{-1}$); 2,6-dimethoxyphenol (2,6-DMP, 500 μM) converted into hydrocoerulignone (ε^{469} = 53,200 $M^{-1}.cm^{-1}$); guaiacol (500 μM) converted into the final product tetraguaiacol (ε^{470} = 26,600 $M^{-1}.cm^{-1}$); Reactive Black 5 (RB5, 100 μM, ε^{600} = 20,000 $M^{-1}.cm^{-1}$) converted into non-chromogenic product $RB5^{ox}$; veratryl alcohol (500 μM) converted into veratraldehyde (ε^{310} = 9,300 $M^{-1}.cm^{-1}$). For testing the manganese peroxidase activity, *Cor*Perox was mixed with Mn(II)SO_4 (1 mM final) in tartrate buffer (50 mM, pH 2.0 to 5.0) and the formation of Mn^{3+}-tartrate complex upon addition of H_2O_2 (100 μM) was followed at 238 nm (ε^{238} = 6,500 $M^{-1}.cm^{-1}$), as previously described[55].

All activities were expressed as Vi/E (s^{-1}), i.e. the initial rate (Vi, μmoles of H_2O_2 consumed per second) divided by the amount of enzyme (in μmoles).

*Cor*Perox stability over time was carried out by monitoring the peroxidase activity of *Cor*Perox samples (50 μM) stored in sodium acetate buffer (50 mM, pH 5.2), at 4°C, in the presence of varying concentrations of $CaCl_2$ (0-500 mM). The peroxidase activity of these samples was measured as described above (final concentration of 0.5 μM *Cor*Perox), using ABTS (500 μM) and H_2O_2 (100 μM) as substrates, in citrate-phosphate buffer (50 mM, pH 4.0), at 23°C.

Michaelis-Menten kinetic parameters of *Cor*Perox were determined by measuring the peroxidase initial rate, as described above, in the presence of ABTS (500 μM) and varying concentrations of H_2O_2 (0-1200 μM), in citrate-phosphate buffer (50 mM, pH 4.0), at 23°C. Experimental data could be fit to the standard Michaelis-Menten equation (residual standard error = 0.019).

AlcOx activation by the peroxidases was assayed by monitoring changes in absorbance at 254 nm upon oxidation of benzyl alcohol (1.5 mM) into benzaldehyde by the CRO (10 nM final concentration), in the presence of varying concentrations of peroxidase (0-1000 nM).

Reactions were carried out in sodium-phosphate buffer (50 mM, pH 7.0), at 23°C, in UV-transparent cuvettes (1 mL reaction volume). The reactions were initiated by addition of the CRO and vigorously mixed by pipetting up and down. The absorbance was measured using an Evolution 201 UV-Vis spectrophotometer (Thermo-Fisher). The concentration of benzaldehyde was calculated as $[Benzaldehyde]_t = (Abs^{254\ nm}_t - Abs^{254\ nm}_{t0})/(\varepsilon^{254}_{benzaldehyde} - \varepsilon^{254}_{BnOH})$, where $\varepsilon^{254}_{benzaldehyde} = 8{,}500\ M^{-1}.cm^{-1}$ and $\varepsilon^{254}_{BnOH} = 150\ M^{-1}.cm^{-1}$.

Gas chromatography (GC) analysis

Enzymatic reactions were carried out in 4 mL-clear borosilicate glass vials closed by screw caps with PTFE septum (500 µL final reaction volume). *Cor*AlcOx (2 µM final) was mixed with *Cor*Perox (2 µM) in sodium phosphate buffer (50 mM, pH 7.0). The reaction was initiated by the addition of octadecanol (0.3 $mg.mL^{-1}$, eq. 1.1 mM final) and the mixture was incubated at 23°C at 190 rpm in an Innova 42R incubator (New Brunswick, USA), during 1 h. Following a previously published protocol[22], the reaction mixture was then acidified by addition of 10 µL HCl (12 M). Products and possible remaining substrate were extracted by adding 500 µL of hexane (containing 1 mM of internal standard dodecane), followed by shaking and centrifugation for 5 min at 3,000 x *g*. The organic layer was transferred into a new vial and analyzed with a GC-2010 Plus apparatus (Shimadzu, Japan) equipped with a flame ionization detector (FID) and a DB-5 capillary column (30 m x 0.25 mm x 0.25 µm; Agilent). Nitrogen (200 kPa) was used as carrier gas. The injector and detector temperatures were set at 250°C. After injection (2 µL sample), the analytes were separated by applying the following temperature program: step 1) from 65°C to 250°C over 9.25 min (i.e. 20°C/min); step 2) plateau at 250°C for 6 min. For quantitation, standard curves of octadecanol, *n*-octadecanal and octadecanoic acid were prepared by following the same procedure.

Electron Paramagnetic Resonance (EPR)

EPR spectra were recorded on frozen solutions (120K) using a Bruker Elexsys E500 spectrometer operating at X-band equipped with a BVT 3000 digital temperature controller. The following acquisition parameters were used: modulation frequency 100 kHz; modulation amplitude 5 G; gain 87 dB; and microwave power, 20 mW. EPR spectra were simulated using the EasySpin toolbox developed for Matlab[56]. *Cor*AlcOx (100 µM final), prepared in sodium phosphate buffer (50 mM, pH 7.0), in the absence or presence of *Cor*Perox (100 µM final), was flash-frozen in liquid nitrogen and continuous-wave EPR spectra were recorded. *Cor*AlcOx and *Cor*Perox were placed in contact for various amount of time (2.5 min, 15 min) before flash-freezing the solution. Controls containing buffer only or the *Cor*Perox were also carried out.

Analysis of cuticular waxes from cucumber cotyledons

Cuticular waxes were extracted from 2-weeks old cotyledons by immersing 6 intact cotyledons for 30 s in chloroform in a glass beaker. Chloroform was evaporated under a stream of nitrogen gas and wax extracts were derivatized using N,O-Bis (trimethylsilyl)trifluoroacetamide (BSTFA) and analyzed by gas chromatography coupled to mass spectrometry (GC-MS) as previously described[57].

Strains and media

Strain 104-T (MAFF240422) of *C. orbiculare* and strain Hoku-1 of *M. oryzae* (MAFF 02-35004) were used as the wild type strains. All strains used in this study are listed in **Supplementary Table 4**[18,36,58–60]. *C. orbiculare* strains were cultured on 3.9% PDA (Nissui) at 24°C in darkness. *M. oryzae* strains were cultured on oatmeal agar (Difco) at 24°C under black light bulbs. For genetic manipulation, *Escherichia coli* DH5α-competent cells were maintained on Luria-Bertani (LB) agar at 37°C. For fungal transformation, *Agrobacterium tumefaciens* C58C1 was maintained on LB agar at 28°C. For Transformations of *C. orbiculare*[18,36] and *M. oryzae*[61,62] were carried out as previously described.

Strain construction

Primers and plasmids used in this study are listed in **Supplementary Table 5**. For construction of *CorAlcOx* deletion strains, 1.1-kb upstream and 1.0-kb downstream flanking sequences and a 1.0-kb fragment of the neomycin-resistance cassette was amplified with the respective primer pairs. For construction of *CorPerox* deletion strains, 1.1-kb upstream and downstream flanking sequences and a 1.4-kb fragment of the hygromycin-resistance cassette was amplified. These three fragments were inserted into linearized pPZP-PvuII using the In-Fusion HD cloning kit (Clontech). The same procedures were used for construction of *M. oryzae* gene deletion strains. For construction of *CorAlcOx-mCherry* and *CorPerox-GFP* gene fusion, a 5.9-kb *CorAlcOx-CorPerox* fragment containing 1.1-kb downstream flanking sequences was inserted into linearized pPZP-PvuII-SUR, and the mCherry and GFP fragments were inserted.
For construction of *CorAlcOx-mCherry* overexpression strains, a 4.0-kb *CorAlcOx-mCherry* fragment containing its 1.1-kb downstream flanking sequence was amplified from pPZP-AlcOx-mCherry-Perox-GFP-S, and fused to linearized pCAMSUR-TEF[63] containing the translation elongation factor promoter of *Aureobasidium pullulans*[64]. The same procedures were used for construction of *CorPerox-GFP* overexpression strains.

Plant infection

Infection assays on detached cucumber leaves (*Cucumis sativus* L. 'Suyo') with conidial suspension (1×10^5 conidia/ml in distilled water) of *C. orbiculare* were performed as previously described[65]. The inoculated leaves were incubated in a humid environment for 5 days at 24°C. Infection assays of *M. oryzae* on detached barley leaves (*Hordeum vulgare* L. 'Nakaizumi-zairai') were performed as previously described[62]. Conidial suspensions (1×10^5 conidia/mL in 0.2% gelatin solution) were spot-inoculated on 7-day-old seedlings, and incubated in a humid box for 5 days at 24°C. All plants were maintained in a growth chamber (16/8 h light/dark cycle, 24°C). For testing the effect of *n*-octadecanal, conidial suspensions (1×10^5 conidia/mL in 10 μM *n*-octadecanal or 1% ethanol) was spotted on detached cucumber leaves, and incubated in a humid environment for 5 days at 24°C.

Microscopy

For observation of appressorium formation of *C. orbiculare* and *M. oryzae*, a conidial suspension (5×10^5 conidia/ml) was placed on a multiwell glass slide or cover glass (Matsunami Glass), respectively. Cells were incubated in a humid box for 24 h at 24°C in the dark. Observation of penetration hyphae on cucumber cotyledons and cellophane membranes were

performed as previously described[18]. Appressorial cytorrhysis assay was conducted based on a previous procedure[58].

A confocal laser scanning microscope LSM900 with Airyscan 2 (Carl Zeiss) equipped with a Plan Apochromat 63×/1.4 Oil DIC objective (Carl Zeiss) was used to acquire confocal microscopic images. Excitation/emission wavelengths were 488 nm/490-556 nm for GFP and 561 nm/565-630 nm for mCherry. Images were acquired and processed using ZEN Software (Version 3.1; Carl Zeiss) and Imaris (Version 9.3.1; Bitplane). For detection of appressorial actin assembly, cells were observed using a Zeiss Axio Imager M2 Upright microscope (Carl Zeiss) equipped with a Plan Apochromat 100× oil immersion lens, an Axio Cam MRm digital camera and excitation/barrier filter set of 595 nm/620 nm for RFP. Images were acquired using Axiovision 4.8. Bright-field microscopy was performed using a Nikon ECLIPSE E600 microscope equipped with a 40× water immersion lens (Nikon) and an OLYMPUS DP74 digital camera system.

Data availability

All data presented in the article and its Extended Data File are available from the corresponding authors upon reasonable request.

References

1. Cooper, J. A. D., Smith, W., Bacila, M. & Medina, H. Galactose Oxidase from *Polyporus circinatus*, Fr.*. *J. Biol. Chem* **234**, 445–448 (1959).
2. Kersten, P. J. & Kirk, T. K. Involvement of a new enzyme, glyoxal oxidase, in extracellular H_2O_2 production by *Phanerochaete chrysosporium*. *J. Bacteriol.* **169**, 2195–2201 (1987).
3. Mathieu, Y. *et al.* Discovery of a Fungal Copper Radical Oxidase with High Catalytic Efficiency toward 5-Hydroxymethylfurfural and Benzyl Alcohols for Bioprocessing. *ACS Catal.* **10**, 3042–3058 (2020).
4. Yin, D. (Tyler) *et al.* Structure–function characterization reveals new catalytic diversity in the galactose oxidase and glyoxal oxidase family. *Nat. Commun.* **6**, 10197 (2015).
5. Lee, S. B. & Suh, M. C. Advances in the understanding of cuticular waxes in *Arabidopsis thaliana* and crop species. *Plant Cell Rep.* **34**, 557–572 (2015).
6. Kamoun, S., Talbot, N. J. & Tofazzal Islam, M. Plant health emergencies demand open science: Tackling a cereal killer on the run. *PLoS Biol.* **17**, 1–6 (2019).
7. Fisher, M. C., Hawkins, N. J., Sanglard, D. & Gurr, S. J. Worldwide emergence of resistance to antifungal drugs challenges human health and food security. *Science.* **360**, 739–742 (2018).
8. Dean, R. *et al.* The Top 10 fungal pathogens in molecular plant pathology. *Mol. Plant Pathol.* **13**, 414–430 (2012).
9. Beimforde, C. *et al.* Estimating the Phanerozoic history of the Ascomycota lineages: Combining fossil and molecular data. *Mol. Phylogenet. Evol.* **78**, 386–398 (2014).
10. Liang, X. *et al.* Pathogenic adaptations of *Colletotrichum* fungi revealed by genome wide gene family evolutionary analyses. *PLoS One* **13**, e0196303 (2018).
11. Ryder, L. S. & Talbot, N. J. Regulation of appressorium development in pathogenic fungi. *Curr. Opin. Plant Biol.* **26**, 8–13 (2015).
12. De Jong, J. C., McCormack, B. J., Smirnoff, N. & Talbot, N. J. Glycerol generates turgor in rice blast. *Nature* **389**, 244–245 (1997).
13. Kubo, Y. & Furusawa, I. Melanin Biosynthesis BT - The Fungal Spore and Disease Initiation in Plants and Animals. in *The Fungal Spore and Disease Initiation in Plants and Animals* (eds. Cole, G. T. & Hoch, H. C.) 205–218 (Springer US, 1991).
14. Chen, Z., Silva, M. C. & Rodriguesjr, C. J. Appressorium Turgor Pressure of *Colletotrichum kahawae* Might Have a Role in Coffee Cuticle Penetration. *Mycologia* **96**, 1199–1208 (2004).
15. Ryder, L. S. *et al.* A sensor kinase controls turgor-driven plant infection by the rice blast fungus. *Nature* **574**, 423–427 (2019).

16. He, M. *et al.* Discovery of broad-spectrum fungicides that block septin-dependent infection processes of pathogenic fungi. *Nat. Microbiol.* **5**, 1565–1575 (2020).
17. Dagdas, Y. F. *et al.* Septin-mediated plant cell invasion by the rice blast fungus, *Magnaporthe oryzae*. *Science.* **336**, 1590–1595 (2012).
18. Kodama, S. *et al.* The morphogenesis-related NDR kinase pathway of *Colletotrichum orbiculare* is required for translating plant surface signals into infection-related morphogenesis and pathogenesis. *PLOS Pathog.* **13**, e1006189 (2017).
19. Rocha, R. O., Elowsky, C., Pham, N. T. T. & Wilson, R. A. Spermine-mediated tight sealing of the *Magnaporthe oryzae* appressorial pore–rice leaf surface interface. *Nat. Microbiol.* **5**, 1472–1480 (2020).
20. Giraldo, M. C. & Valent, B. Filamentous plant pathogen effectors in action. *Nat. Rev. Microbiol.* **11**, 800–814 (2013).
21. Djamei, A. *et al.* Metabolic priming by a secreted fungal effector. *Nature* **478**, 395–398 (2011).
22. Ribeaucourt, D. *et al.* Controlled Oxidation of Long-Chain Primary Aliphatic Alcohols by a Fungal Copper-Radical Alcohol Oxidase. *ACS Sustain. Chem. Eng.* **9**, 4411–4421 (2021).
23. Parikka, K. & Tenkanen, M. Oxidation of methyl α-D-galactopyranoside by galactose oxidase: products formed and optimization of reaction conditions for production of aldehyde. *Carbohydr. Res.* **344**, 14–20 (2009).
24. Forget, S. M., Xia, F. R., Hein, J. E. & Brumer, H. Determination of biocatalytic parameters of a copper radical oxidase using real-time reaction progress monitoring. *Org. Biomol. Chem.* **18**, 2076–2084 (2020).
25. Zerva, A., Christakopoulos, P. & Topakas, E. Characterization and application of a novel class II thermophilic peroxidase from *Myceliophthora thermophila* in biosynthesis of polycatechol. *Enzyme Microb. Technol.* **75**–**76**, 49–56 (2015).
26. O'Connell, R. J. *et al.* Lifestyle transitions in plant pathogenic *Colletotrichum* fungi deciphered by genome and transcriptome analyses. *Nat. Genet.* **44**, 1060–1065 (2012).
27. Gan, P. *et al.* Comparative genomic and transcriptomic analyses reveal the hemibiotrophic stage shift of *Colletotrichum* fungi. *New Phytol.* **197**, 1236–1249 (2013).
28. Dong, Y. *et al.* Global Genome and Transcriptome Analyses of *Magnaporthe oryzae* Epidemic Isolate 98-06 Uncover Novel Effectors and Pathogenicity-Related Genes, Revealing Gene Gain and Lose Dynamics in Genome Evolution. *PLoS Pathog.* **11**, 1–30 (2015).
29. Shimizu, M. *et al.* RNA-Seq of in planta-expressed *Magnaporthe oryzae* genes identifies MoSVP as a highly expressed gene required for pathogenicity at the initial stage of infection. *Mol. Plant Pathol.* **20**, 1682–1695 (2019).
30. Rodriguez-Lopez, J. N., Smith, A. T. & Thorneley, R. N. F. Role of Arginine 38 in Horseradish Peroxidase. A critical residue for substrate binding and catalysis. *J. Biol. Chem.* **271**, 4023–4030 (1996).
31. Bissaro, B., Varnai, A., Røhr, Å. K. & Eijsink, V. G. H. Oxidoreductases and reactive oxygen species in lignocellulose biomass conversion. *Microbiol. Mol. Biol. Rev.* **4**, (2018).
32. Ayuso-Fernández, I., Ruiz-Dueñas, F. J. & Martínez, A. T. Evolutionary convergence in lignin-degrading enzymes. *Proc. Natl. Acad. Sci. U. S. A.* **115**, 6428–6433 (2018).
33. Oide, S., Tanaka, Y., Watanabe, A. & Inui, M. Carbohydrate-binding property of a cell wall integrity and stress response component (WSC) domain of an alcohol oxidase from the rice blast pathogen *Pyricularia oryzae*. *Enzyme Microb. Technol.* **125**, 13–20 (2019).
34. Ito, N. *et al.* Novel thioether bond revealed by a 1.7 Å crystal structure of galactose oxidase. *Nature* **350**, 87–90 (1991).
35. Pham, C. L. L. *et al.* Self-assembly of MPG1, a hydrophobin protein from the rice blast fungus that forms functional amyloid coatings, occurs by a surface-driven mechanism. *Sci. Rep.* **6**, 25288 (2016).
36. Fukada, F. & Kubo, Y. *Colletotrichum orbiculare* Regulates Cell Cycle G1/SProgression via a Two-Component GAP and a GTPase to Establish Plant Infection. *Plant Cell* **27**, 2530–2544 (2015).
37. Leuthner, B. *et al.* A H_2O_2-producing glyoxal oxidase is required for filamentous growth and pathogenicity in *Ustilago maydis*. *Mol. Genet. Genomics* **272**, 639–650 (2005).
38. Chaplin, A. K. *et al.* GlxA is a new structural member of the radical copper oxidase family and is required for glycan deposition at hyphal tips and morphogenesis of *Streptomyces lividans*. *Biochem. J.* **469**, 433–444 (2015).
39. Liu, W. *et al.* Multiple plant surface signals are sensed by different mechanisms in the rice blast fungus for appressorium formation. *PLoS Pathog.* **7**, (2011).
40. Kolattukudy, P. E., Rogers, L. M., Li, D., Hwang, C. S. & Flaishman, M. A. Surface signaling in pathogenesis. *Proc. Natl. Acad. Sci. U. S. A.* **92**, 4080–4087 (1995).
41. Pickl, M., Fuchs, M., Glueck, S. M. & Faber, K. The substrate tolerance of alcohol oxidases. *Appl. Microbiol. Biotechnol.* **99**, 6617–6642 (2015).
42. Morin, E. *et al.* Comparative genomics of *Rhizophagus irregularis*, *R. cerebriforme*, *R. diaphanus* and *Gigaspora rosea* highlights specific genetic features in Glomeromycotina. *New Phytol.* **222**, 1584–1598

(2019).
43. Wattam, A. R. *et al.* PATRIC, the bacterial bioinformatics database and analysis resource. *Nucleic Acids Res.* **42**, D581–D591 (2014).
44. Katoh, K. & Standley, D. M. MAFFT Multiple Sequence Alignment Software Version 7: Improvements in Performance and Usability. *Mol. Biol. Evol.* **30**, 772–780 (2013).
45. Castresana, J. Selection of Conserved Blocks from Multiple Alignments for Their Use in Phylogenetic Analysis. *Mol. Biol. Evol.* **17**, 540–552 (2000).
46. Stamatakis, A. RAxML version 8: a tool for phylogenetic analysis and post-analysis of large phylogenies. *Bioinformatics* **30**, 1312–1313 (2014).
47. Zámocký, M., Janeček, Š. & Obinger, C. Fungal Hybrid B heme peroxidases – unique fusions of a heme peroxidase domain with a carbohydrate-binding domain. *Sci. Rep.* **7**, 9393 (2017).
48. Katoh, K., Rozewicki, J. & Yamada, K. D. MAFFT online service: Multiple sequence alignment, interactive sequence choice and visualization. *Brief. Bioinform.* **20**, 1160–1166 (2018).
49. Letunic, I. & Bork, P. Interactive Tree of Life (iTOL) v4: Recent updates and new developments. *Nucleic Acids Res.* **47**, 256–259 (2019).
50. Kelley, L. A., Mezulis, S., Yates, C. M., Wass, M. N. & Sternberg, & M. J. E. The Phyre2 web portal for protein modeling, prediction and analysis. *Nat. Protoc.* **10**, 845–858 (2016).
51. Hebditch, M. & Warwicker, J. Web-based display of protein surface and pH-dependent properties for assessing the developability of biotherapeutics. *Sci. Rep.* **9**, 1–9 (2019).
52. Kyte, J. & F.Doolittle, R. A simple method for displaying the hydropathic character of a protein. *J. Mol. Biol.* **157**, 105–132 (1982).
53. Haon, M. *et al.* Recombinant protein production facility for fungal biomass-degrading enzymes using the yeast *Pichia pastoris*. *Front. Microbiol.* **6**, 1–12 (2015).
54. Bradford, M. M. A rapid and sensitive method for the quantitation of microgram quantities of protein utilizing the principle of protein-dye binding. *Anal. Biochem.* **72**, 248–254 (1976).
55. Martínez, M. J., Ruiz-Dueñas, F. J., Guillén, F. & Martínez, Á. T. Purification and catalytic properties of two manganese peroxidase isoenzymes from *Pleurotus eryngii*. *Eur. J. Biochem.* **237**, 424–432 (1996).
56. Stoll, S. & Schweiger, A. EasySpin, a comprehensive software package for spectral simulation and analysis in EPR. *J. Magn. Reson.* **178**, 42–55 (2006).
57. Ménard, R. *et al.* Histone H2B monoubiquitination is involved in the regulation of cutin and wax composition in *Arabidopsis thaliana*. *Plant Cell Physiol.* **55**, 455–466 (2014).
58. Tanaka, S. *et al. Saccharomyces cerevisiae* SSD1 orthologues are essential for host infection by the ascomycete plant pathogens *Colletotrichum lagenarium* and *Magnaporthe grisea*. *Mol. Microbiol.* **64**, 1332–1349 (2007).
59. Kimura, M., Izawa, K., Yoneyama, K., Arie, T. & Kamakura, T. A Novel Transformation System for *Pyricularia Oryzae*: Adhesion of Regenerating Fungal Protoplasts to Collagen-Coated Dishes. *Biosci. Biotechnol. Biochem.* **59**, 1177–1180 (1995).
60. Ishida, N. & Akai, S. Relation of Temperature to Germination of Conidia and Appressorium Formation in *Colletotrichum lagenarium*. *Mycologia* **61**, 382–386 (1969).
61. Chen, X.-L., Yang, J. & Peng, Y.-L. Large-scale insertional mutagenesis in *Magnaporthe oryzae* by *Agrobacterium tumefaciens*-mediated transformation. *Methods Mol. Biol. (N. Y.)* **722**, 213–224 (2011).
62. Fukada, F., Kodama, S., Nishiuchi, T., Kajikawa, N. & Kubo, Y. Plant pathogenic fungi *Colletotrichum* and *Magnaporthe* share a common G 1 phase monitoring strategy for proper appressorium development. *New Phytol.* **222**, 1909–1923 (2019).
63. Saitoh, K. *et al.* Construction of a Binary Vector for Knockout and Expression Analysis of Rice Blast Fungus Genes. *Biosci. Biotechnol. Biochem.* **72**, 1380–1383 (2008).
64. Wymelenberg, A. J. Vanden, Cullen, D., Spear, R. N., Schoenike, B. & Andrews, J. H. Expression of green fluorescent protein in *Aureobasidium pullulans* and quantification of the fungus on leaf surfaces. *Biotechniques* **23**, 686–690 (1998).
65. Tsuji, G., Fujii, S., Tsuge, S., Shiraishi, T. & Kubo, Y. The *Colletotrichum lagenariu* Ste12-like gene CST1 is essential for appressorium penetration. *Mol. Plant. Microbe. Interact.* **16**, 315—325 (2003).

Acknowledgments

We thank Drs. Morin and Lebreton (INRAE Nancy, France) for allowing us to use their in-house tool "Genocomp" for species tree construction. We thank Dr. Nakayashiki (Kobe University, Japan) for providing Barley seeds and Pamela Gan (RIKEN-CSRS, Japan) for sharing unpublished transcriptome data. This study was supported by the “Agence Nationale de la Recherche” and by the Natural Sciences and Engineering Research Council of Canada

through the ANR-NSERC project “FUNTASTIC” (ANR-17-CE07-0047, STPGP 493781-16). We are grateful to MANE & Fils and the “Association Nationale Recherche Technologie” (ANRT) for funding the Ph.D. fellowship of D.R. (grant no. 2017/1169). Work in Japan was supported by the Japan Society for the Promotion of Science Grants-in-Aid for Scientific Research – KAKENHI, Grant Numbers 15H05780 and 20H02989 to Y.K., and 20K15529 to S.K.

Author contributions

B.B., S.K., R.O’C., M.L., Y.K., and J.G.B. conceived the work. J.G.B and Y.K. coordinated the study. B.B., S.K., H.H., D.R., A.J.S., R.O’C., M.L., Y.K., and J.G.B. designed the experiments. B.B., S.K., H.H., D.R., M.H., S.G., F.B., and A.J.S. performed the experiments. B.B., S.K., H.H., D.R., A.J.S., S.M.F., H.B., M.N.R., R.O’C., M.L., Y.K., and J.G.B. analyzed the data. B.B., S.K., Y.K., and J.G.B. wrote the original draft with review and editing from M.L., H.B., and R.O’C. All authors have approved the final version of the paper.

Competing interests

The authors declare no competing interests.

Additional information

Extended Data contains Extended Data Figs 1 to 10, Supplementary Tables 1 to 5, Supplementary Movie 1, and a Supplementary References list.

Supplementary Files

This is a list of supplementary files associated with this preprint. Click to download.

- BissaroKodamaNatChemBiolExtendedDatavf.pdf
- SupplementalMovie1SK.mp4